

Predicting the Dimits shift through reduced mode tertiary instability analysis in a strongly driven gyrokinetic fluid limit

Axel Hallenbert^{1†} and Gabriel G. Plunk¹

¹Max-Planck-Institut für Plasmaphysik, D-17491 Greifswald, Germany

(Received xx; revised xx; accepted xx)

The tertiary instability is believed to be important for governing magnetised plasma turbulence under conditions of strong zonal flow generation, near marginal stability. In this work, we investigate its role for a collisionless strongly driven fluid model, self-consistently derived as a limit of gyrokinetics. It is found that a region of absolute stability above the linear threshold exists, beyond which significant nonlinear transport rapidly develops. While within this range a complex pattern of transient zonal evolution is observed before a stable profile is found, the Dimits transition itself is found to coincide with a tertiary instability threshold so long as linear effects are included. Through a simple and readily extendable procedure tracing its origin to St-Onge (2017), the stabilising effect of the typical zonal profile can be approximated and the accompanying reduced mode estimate is found to be in good agreement with nonlinear simulations.

1. Introduction

Experimental fusion devices exhibit significantly higher transport than neoclassical predictions. The additional anomalous transport arises as a result of gyroscale micro-turbulence driven by various instabilities (Liewer 1985), such as the ion temperature gradient (ITG) mode (Choi & Horton 1980; Horton *et al.* 1981; Connor & Wilson 1994) or the trapped electron mode (Kadomtsev & Pogutse 1970; Nordman *et al.* 1990). Moreover, the turbulent transport associated with these instabilities is very stiff. Thus, once instability is present, even a small increase in the plasma gradients will drastically increase the transport, effectively freezing the gradients in place and restricting device performance (Ryter *et al.* 2011). This picture is expected to continue to hold for future fusion devices, and so being able to predict when this transport threshold is reached becomes of key importance to predict overall behaviour and performance. This is of obvious importance for the understanding and design of experiments, and might be useful for optimisation, especially of stellarator devices, which possess a large degree of freedom in the configuration of their magnetic geometries.

Naively, one might expect that the transport threshold should coincide with the linear instability threshold, since fundamentally these extract free energy from the plasma gradients to drive the turbulent transport. However, instead it is found that finite transport actually commences at significantly steeper gradients than this. This apparent discrepancy traces its origin to self-generated poloidal zonal flows. Once the primary drift waves reach sufficient magnitude, such flows naturally arise through nonlinear interactions in what is known as a secondary instability. As the zonal flows become strong enough, they can then, in turn, nonlinearly stabilise the primary instability by

† Email address for correspondence: axel.hallenbert@ipp.mpg.de

shearing drift waves and decreasing their correlation length. Because the zonal flows have a Landau-undamped component (Rosenbluth & Hinton 1998) they can, close to marginal stability and in the absence of collisions, persist for such a long time that the effective transport nearly vanishes. This is known as the Dimits regime, and the effective upshift of the critical gradient, i.e. the difference between the linear critical gradient and the observed critical gradient for the onset of turbulence, is known as the Dimits shift, both after their discoverer (Dimits *et al.* 2000).

Despite the qualitative picture of the Dimits shift as just outlined being somewhat firmly established, there are still some key features which are poorly understood. Thus a general quantitative prediction of the Dimits shift has proven elusive. To describe the ITG turbulence typically observed in experiments, it is necessary to employ full gyrokinetics to retain all relevant physics (Catto 1978; Frieman 1982; Abel *et al.* 2013). This however is a highly complex kinetic system, and attempting to thoroughly account for all the possibly relevant features necessary for a full description of the Dimits shift has proved a daunting task. Instead much research has been undertaken for simpler systems which are analytically tractable, typically of the Hasegawa-Mima-Wakatani family (Hasegawa & Mima 1978; Hasegawa & Wakatani 1983), in order to gain the insight necessary to parse key features which could render the gyrokinetic problem solvable.

Many different features have been observed which could prove to be of relevance for the full problem. These include, but are not limited to, coupling to subdominant modes at unstable scales (Makwana *et al.* 2014), time-coherent localised soliton structures known as ferdinons (van Wyk *et al.* 2016, 2017; Ivanov *et al.* 2020), zonal-drift predator-prey-type interactions (Kobayashi & Rogers 2012; Berionni & Gürcan 2011), or the ability of a turbulent momentum flux to tear down or build up a decaying zonal profile (Kim & Diamond 2002; Ivanov *et al.* 2020). One feature, however, which crops up repeatedly in these studies is that instability causing drift waves to arise from an initially zonally dominated state that is known as the tertiary instability (Rogers *et al.* 2000).

Despite seemingly being a natural candidate to explain the observed Dimits shift, based on findings from simpler systems, the importance for the Dimits shift of the tertiary instability has nevertheless been a topic of debate within the literature. St-Onge (2017) and Zhu *et al.* (2020a) for example based accurate predictions upon it, while Li & Diamond (2018), Rath *et al.* (2018), and Ivanov *et al.* (2020) on the contrary reported finding it unimportant. To help rectify this confusion, in this paper we will thus attempt to shed some light on the tertiary mode in the Dimits regime by investigating its relevance for the Dimits transition in a strongly driven fluid system directly derived from gyrokinetics.

In our investigations we will find that, just like Zhu *et al.* (2020a) stressed, in order to properly capture the behaviour of the tertiary instability in the marginally stable regime, the linear drive cannot be neglected. The tertiary instability should not be treated as a purely Kelvin-Helmholtz-like (KH) instability, but instead as a modified primary instability that includes such terms. Then the tertiary instability alone seems sufficient to encapsulate the Dimits transition for the system under consideration. This is despite the fact that this system is ostensibly similar to the one recently studied by Ivanov *et al.* (2020), where the opposite case was found to hold, a discrepancy arising from the lack of collisional zonal flow damping. Finally we will see that a reduced mode scheme to approximate the tertiary instability can yield a simple but effective prediction (within 15-30%). Furthermore this scheme seems readily extendable to more difficult systems, including gyrokinetics itself, which will be the subject of an upcoming publication.

This paper is outlined as follows. The strongly driven gyrofluid-system will first be derived in Section 2 and its key features will then be presented in 3. Next we will in

turn describe each of the present instabilities of the primary-secondary-tertiary paradigm (see Kim & Diamond 2002), noting their effects on the system as a whole. Guided by direct simulations presented in Section 4, we will then home in further on the tertiary instability in Section 5. There we will show that it can be employed to arrive at a very simple Dimits shift estimate, related to the one of St-Onge (2017), which could prove to be broadly applicable for other non-collisional systems as well. Finally we will conclude with a brief summary and discussion in Section 6.

2. Basic model

The Dimits shift was originally observed in, and is of most experimental relevance for, full gyrokinetic simulations of tokamaks (Dimits *et al.* 2000). However, the intrinsic kinetic nature of this system makes analytical treatment of even just the tertiary instability intractable. Investigations have therefore focused on simplified problems, hoping to find insights which can be extrapolated to the more complete problem. Naturally these models all fail to capture much of the physics of the full gyrokinetic system because of their simplicity, possibly raising concerns about how valid this extrapolation will be. Therefore we will here present another self-consistently closed gyrofluid system in two spatial dimensions, in the hope that it may prove yet another useful stepping stone to solidify and clarify the emerging picture of the Dimits shift when proceeding towards the full gyrokinetic problem.

To arrive at the system of interest one starts from the usual electrostatic collisionless gyrokinetic equation in Fourier space, which we in the vein of Plunk *et al.* (2014) express in non-dimensional form as

$$\left(\frac{\partial}{\partial t} + i\tilde{\omega}_d\right) h_{\mathbf{k}} + \{\Phi, h\}_{\mathbf{k}} = \left(\frac{\partial}{\partial t} + i\tilde{\omega}_*\right) \Phi_{\mathbf{k}} f_0. \quad (2.1)$$

Here f_0 is the ion Maxwellian mean distribution with thermal velocity $v_T = \sqrt{2T/m}$, h is the non-adiabatic part of the ion fluctuations δf_i , and Φ is the gyroaveraged electrostatic potential. The gyroaverage in Fourier space, in turn, is encapsulated by the Bessel function of the first kind $J_0 = J_0(\sqrt{2}k_{\perp}w_{\perp})$, where $w = v/v_T$, through $\Phi_{\mathbf{k}} = J_0\varphi_{\mathbf{k}}$, and the Fourier space Poisson bracket is given by

$$\{a, b\}_{\mathbf{k}} = \sum_{\mathbf{k}_1, \mathbf{k}_2} (k_{1y}k_{2x} - k_{1x}k_{2y}) a_{\mathbf{k}_1} b_{\mathbf{k}_2} \delta_{\mathbf{k}, \mathbf{k}_1 + \mathbf{k}_2}, \quad (2.2)$$

where the x - and y -coordinates are the radial and poloidal coordinates respectively. After the introduction of a reference length scale L_{ref} , the spatial and temporal dimensions are normalised to the typical ion gyroradius ρ and the streaming time v_T/L_{ref} respectively, so that $\varphi = q\phi L_{\text{ref}}/T\rho$ is the dimensionless electrostatic potential. Furthermore β is assumed small so that $\nabla \ln B \approx \mathbf{b} \cdot \nabla \mathbf{b}$, which enables the velocity-dependent diamagnetic and magnetic drift frequencies

$$\tilde{\omega}_* = \omega_* \left(1 + \eta \left(w^2 - \frac{3}{2}\right)\right) \quad \text{and} \quad \tilde{\omega}_d = \omega_d \left(w_{\parallel}^2 + \frac{w_{\perp}^2}{2}\right) \quad (2.3)$$

to be succinctly expressed entirely in terms of the four parameters

$$\omega_* = \frac{k_y L_{\text{ref}}}{\sqrt{2}L_n} = \omega_{*0} k_y, \quad \omega_d = \frac{\sqrt{2}k_y L_{\text{ref}}}{R} = \omega_{d0} k_y, \quad \eta = \frac{L_n}{L_T}, \quad \text{and} \quad \tau = \frac{T_i}{T_e}, \quad (2.4)$$

from the electron/ion temperatures $T_{e/i}$ and the characteristic density, temperature, and

magnetic curvature lengths

$$L_n = \left(\frac{d \ln n}{dx} \right)^{-1}, \quad L_T = \left(\frac{d \ln T}{dx} \right)^{-1}, \quad \text{and} \quad R = \left(\frac{d \ln B}{dx} \right)^{-1} \quad (2.5)$$

(all three negative by our convention).

To couple the potential φ to the ion gyrocenter distribution h and close the system, the electrons are taken to follow a modified adiabatic response such that the quasineutrality condition becomes

$$\int d^3 \mathbf{v} J_0 h = n(1 + \tau \hat{\alpha}) \varphi, \quad (2.6)$$

where $\hat{\alpha}$ is the operator

$$\hat{\alpha} a = a(x, y) - \frac{1}{L_y} \int_0^{L_y} a(x, y) dy, \quad (2.7)$$

i.e. an operator that is zero when acting on purely zonal $\mathbf{E} \times \mathbf{B}$ modes with $k_y = 0$, and unity otherwise.

To serve our purpose of studying the Dimits shift, the gyrokinetic equation in the form of (2.1) clearly neglects both parallel variations and collisions. The former omission constitutes a considerable simplification from a spatially 3D to a spatially 2D system, but necessarily excludes the ITG slab mode. Instead the focus becomes a local description of the well-known bad-curvature-driven toroidal ITG instability (Beer 1995), which seems to be of most relevance for the Dimits transition (Dimits *et al.* 2000). The second omission is similarly made because, should collisions be included, their presence significantly muddles the waters. This is because a wide range of zonal flow behaviour then manifests, including bursty patterns (see Berionni & Gürçan 2011) or non-quasistatic flows (see Kobayashi & Rogers 2012), so that it can become somewhat difficult to identify a clear Dimits transition or even reliably define the Dimits shift. However, in their absence, Landau-undamped Rosenbluth-Hinton states (Rosenbluth & Hinton 1998) can produce static zonal flow states with zero transport, in principle (only limited by the finite simulation time available to find such a state) providing a clear cut distinction between systems within and outside the Dimits regime.

Employing a subsidiary ordering such that

$$\frac{\partial_t}{\eta \omega_*} \sim \frac{\omega_d}{\omega_*} \sim k_\perp^2 \sim \frac{\tilde{\varphi}^2}{\varphi^2} \sim \frac{\tilde{h}^2}{h^2} \sim \frac{1}{\eta} \ll 1, \quad (2.8)$$

where the gyrophase-independent response and potential have been split into their zonal and nonzonal components like

$$\bar{h} = (1 - \hat{\alpha}) h, \quad \tilde{h} = \hat{\alpha} h, \quad \bar{\varphi} = (1 - \hat{\alpha}) \varphi, \quad \tilde{\varphi} = \hat{\alpha} \varphi, \quad (2.9)$$

one finds that it is necessary to employ the ordering

$$T_\perp = \int d^3 w w_\perp^2 h \sim T_\parallel = \int d^3 w w_\parallel^2 h \sim \eta \int d^3 w h \quad (2.10)$$

to balance the dominant $\eta \tilde{\omega}_*$ -term in the gyrokinetic equation, since this term has a vanishing density moment but a non-vanishing temperature moment. With this ordering one then finds that the gyrokinetic moment hierarchy self-consistently closes at second

order, resulting in the equation system:

$$\begin{aligned} & \frac{\partial \tau \tilde{\varphi}_{\mathbf{k}}}{\partial t} + \{\tilde{\varphi}, \tau \tilde{\varphi}\}_{\mathbf{k}} + \left\{ \nabla_{\perp}^2 \tilde{\varphi}, \tilde{T}_{\perp} \right\}_{\mathbf{k}} - k_{\perp}^2 \left\{ \tilde{\varphi}, \tilde{T}_{\perp} \right\}_{\mathbf{k}} - \left\{ \tilde{\varphi}, \nabla_{\perp}^2 \tilde{T}_{\perp} \right\}_{\mathbf{k}} \\ & = i\omega_* (1 - \eta k_{\perp}^2) \tilde{\varphi}_{\mathbf{k}} - i\omega_d \left(\frac{\tilde{T}_{\parallel \mathbf{k}}}{2} + \frac{\tilde{T}_{\perp \mathbf{k}}}{4} \right) - D_{\mathbf{k}} \tau \tilde{\varphi}_{\mathbf{k}}, \end{aligned} \quad (2.11)$$

$$\frac{\partial k_{\perp}^2 \tilde{\varphi}_{\mathbf{k}}}{\partial t} + \left\{ \nabla_{\perp}^2 \tilde{\varphi}, \tilde{T}_{\perp} \right\}_{\mathbf{k}} - k_{\perp}^2 \left\{ \tilde{\varphi}, \tilde{T}_{\perp} \right\}_{\mathbf{k}} - \left\{ \tilde{\varphi}, \nabla_{\perp}^2 \tilde{T}_{\perp} \right\}_{\mathbf{k}} = 0, \quad (2.12)$$

$$\frac{\partial \tilde{T}_{\perp \mathbf{k}}}{\partial t} + \left\{ \tilde{\varphi}, \tilde{T}_{\perp} \right\}_{\mathbf{k}} = \frac{i\omega_* \eta \tilde{\varphi}_{\mathbf{k}}}{2} - D_{\mathbf{k}} \tilde{T}_{\perp \mathbf{k}}, \quad (2.13)$$

$$\frac{\partial \tilde{T}_{\parallel \mathbf{k}}}{\partial t} + \left\{ \tilde{\varphi}, \tilde{T}_{\parallel} \right\}_{\mathbf{k}} = \frac{i\omega_* \eta \tilde{\varphi}_{\mathbf{k}}}{4} - D_{\mathbf{k}} \tilde{T}_{\parallel \mathbf{k}}. \quad (2.14)$$

Here an ad hoc damping operator D acting on the non-zonal components, to be further discussed in Section 3.1, has been added to compensate for the loss of collisionless damping (Landau 1946) that occurs upon taking moments of the gyrokinetic equation. Note that the system consists of one zonal field $\tilde{\varphi}$ and three non-zonal fields $\tilde{\varphi}$, \tilde{T}_{\perp} , \tilde{T}_{\parallel} ; the zonal components of the temperature do not enter.

Some comments about this ordering and its resulting system are now in order. First, apart from the additional separation of the zonal and nonzonal components in the ordering scheme, this corresponds to a strongly driven limit with a high temperature gradient feeding a strong ITG instability and causing short wavelength turbulence to be dominant, previously studied in its linear (Plunk *et al.* 2014) and nonlinear (Plunk *et al.* 2012) limits separately. The specific additional zonal/nonzonal separation within the ordering scheme is necessary for a consistent closure including both linear and nonlinear interactions. Beyond this it also encapsulates the fact that only the former are so called modes of minimal inertia (Diamond *et al.* 2005), being easily excited due to the density shielding of the adiabatic electron response. Furthermore, being Landau-undamped they can persist for long times, and so they are observed to be comparatively strong.

Secondly, all the present nonlinear terms affecting the drift waves involve zonal flows. Farrell & Ioannou (2009) have already shown that, beyond the Dimits regime, simple systems (specifically Hasegawa-Wakatani) can exhibit all relevant physics despite lacking driftwave-driftwave interactions. Thus it may be unsurprising that we here will find that the same can be true inside the Dimits regime. Beyond this we note that the full nonlinear interaction is asymmetrical between the different fields. While the governing equations for the non-zonal fields all include the typical $\mathbf{E} \times \mathbf{B}$ -advection nonlinear $\{\tilde{\varphi}, \cdot\}$ -term, both the zonal and nonzonal potentials $\tilde{\varphi}$ and $\tilde{\varphi}$ are affected by an additional set of nonlinear diamagnetic drift FLR terms coupling them to \tilde{T}_{\perp} .

Thirdly, barring the splitting of the temperature moment into its separate parallel and perpendicular components, the nonlinear interaction is the same as Plunk *et al.* (2012). By a trivial modification of the results therein, the electrostatic energy conserved by the nonlinear interactions in 2.11-2.14 is therefore readily found to be given by

$$E_{\varphi} = E_{\tilde{\varphi}} + E_{\tilde{\varphi}} = \frac{1}{2L_x L_y} \int |\nabla \tilde{\varphi}|^2 dx dy + \frac{1}{2L_x L_y} \int \tau \tilde{\varphi}^2 dx dy. \quad (2.15)$$

Finally, this strongly driven system is clearly formally far from the usual marginally unstable Dimits regime by virtue of its ordering, and one might question its relevance when investigating the Dimits shift. However, with a sufficiently large D , marginal stability can be reinstated and a clear Dimits regime emerges. This system may thus act

as a stepping stone, since its self-consistent closure means that the nonlinear interaction should closely resemble that of full gyrokinetics, at least in its range of validity. Indeed it bears much resemblance to another, but highly collisional, gyrokinetic fluid limit recently studied by Ivanov *et al.* (2020), differing beyond the obvious collisional difference in mainly three ways: i) the lack of collisions means that the parallel and perpendicular temperature moments fail to equilibrate into a single isotropic temperature, ii) the nonlinear driftwave-driftwave interaction becomes too small to be of relevance, iii) the zonal temperature perturbations cease to be dynamically relevant.

3. Key features

3.1. Primary Instability

To arrive at a linear dispersion relation for the modes the system of (2.11)-(2.14), plane wave solutions proportional to $\exp(\lambda_{\mathbf{k}}t + i\mathbf{k} \cdot \mathbf{r})$ are postulated, where $\lambda_{\mathbf{k}}$ can be split into the growth rate $\gamma_{\mathbf{k}}$ and frequency $\omega_{\mathbf{k}}$ according to $\lambda_{\mathbf{k}} = \gamma_{\mathbf{k}} - i\omega_{\mathbf{k}}$. A straightforward linear instability calculation then reveals the presence of a pure temperature mode (where $\tilde{\varphi}_{\mathbf{k}} = 0$, but \tilde{T}_{\perp} and \tilde{T}_{\parallel} are nonzero) which is strictly damped,

$$\gamma_{\mathbf{k}}^T = -D_{\mathbf{k}}, \quad (3.1)$$

and two modes with the expected dispersion relations

$$\lambda_{\mathbf{k}}^{\pm} = \gamma_{\mathbf{k}}^{\pm} - i\omega_{\mathbf{k}}^{\pm} = -D_{\mathbf{k}} + i\omega_{*} \frac{1 - \eta k_{\perp}^2}{2\tau} \pm \frac{1}{2\tau} \sqrt{\eta\tau\omega_{*}\omega_d - \omega_{*}^2(1 - \eta k_{\perp}^2)^2} \quad (3.2)$$

of the toroidal ITG mode inherent to the ordering (2.8) (Plunk *et al.* 2014).

Because D generally introduces only a k -dependent shift in γ towards lower values, it is useful to first consider $D = 0$. Remembering that the definitions of ω_{*} and ω_d include a factor k_y , several features are readily apparent. The most unstable mode is as expected the purely radial streamer with $k_x = q = 0$ satisfying

$$k_y^2 = p^2 = \frac{1}{3\eta} \left(2 + \sqrt{1 + \frac{3\eta\tau\omega_d}{\omega_{*}}} \right). \quad (3.3)$$

Note here the introduction of q and p which will henceforth be used for poloidal and radial wavenumbers respectively. Now, when (3.3) is inserted into (3.2) it gives the expected bad curvature ITG instability scaling (see Beer 1995)

$$\gamma_{\mathbf{k}}^+ \propto \frac{k_y}{\sqrt{\tau RL_T}}, \quad (3.4)$$

when the correction term under the root is taken to be small. When this term on the other hand is sufficiently large, the growth rate passes through zero. Thus we find that only the wavenumbers within the annulus

$$\frac{1}{\eta} \left(1 - \sqrt{\frac{\eta\tau\omega_d}{\omega_{*}}} \right) < k_{\perp}^2 < \frac{1}{\eta} \left(1 + \sqrt{\frac{\eta\tau\omega_d}{\omega_{*}}} \right) \quad (3.5)$$

can be unstable. Here we see that η pushes the instability to larger scales, while $\tau\omega_d/\omega_{*}$ controls the narrowness of the instability annulus and whether large scales are damped or not (indeed as $\eta\tau\omega_d/\omega_{*}$ exceeds 1, the annulus becomes a disk), see Figure 1. Clearly (3.3) and (3.5) sets the energy injection scale to be $\sqrt{(1/\eta)}$ in accordance with the subsidiary ordering 2.8, which is therefore justified a posteriori.

Examining the linear growth rate (3.2) it is clear that, as long as there exists bad

magnetic curvature providing finite ω_d , and in the absence of artificial dissipation $D_{\mathbf{k}}$, the primary instability is present at $\eta k_{\perp}^2 = 1$ given any arbitrarily small density and temperature gradients. Furthermore all arbitrarily small scales are completely undamped and so can act as a reservoir of energy. Numerically, this means that even though every unstable $\lambda_{\mathbf{k}}^+$ -mode in the injection range is accompanied by a damped $\lambda_{\mathbf{k}}^-$ -mode, without D the system could nonlinearly diverge while exhibiting large-scale energy pileup typical of 2D-turbulence with its inverse enstrophy cascade (Kraichnan 1967; Qian 1986; Terry 2004). In 3D turbulence this is prevented by a scale balance of parallel streaming and turbulence known as critical balance (Barnes *et al.* 2011), but no such mechanism is available here.

Given what was just outlined, in order to prevent nonphysical absolute instability and the excitation of arbitrary small or large scales, the necessity of including some kind of D is apparent. Physically this is meant to represent the Landau-type damping present in weakly collisional gyrokinetics but which was lost upon only considering its moments to arrive at (2.11)-(2.14). Though our ordering (2.8) implies that the kinetic damping is small, it is nevertheless non-zero and so dynamically relevant, particularly for the marginally stable small scales it firmly stabilises (see Sugama 1999).

With the inclusion of D , we can arrive at a linear instability threshold for the temperature gradient when D is constant. Remembering that ω_* and ω_d both include a factor k_y , we find upon inserting (3.3) into (3.2) and setting the result to 0, that it becomes a condition on $\eta(D)$ for the most unstable mode to be marginally stable. Its $\eta > 0$ -solution is denoted by

$$\eta^0 = \frac{8\tau D^2}{9\omega_{d0}\omega_{*0}} \quad (3.6)$$

and it is found that, for η larger than this value, γ^+ increases monotonically with η . When $D_{\mathbf{k}}$ is allowed to vary, (3.6) is slightly modified because the wavenumber of the most unstable mode shifts away from (3.3), but this monotonicity continues to hold. Therefore, for some η^0 (typically close to (3.6) with $D = D_p$) we have a robust absolute instability condition

$$\eta > \eta^0. \quad (3.7)$$

Returning again to the unstable mode it naturally includes both potential and temperature perturbations, so upon inserting (3.2) into (2.11)-(2.14) the ratio between the two can be calculated to be

$$\frac{\tilde{\varphi}_{\mathbf{k}}}{\tilde{T}_{\perp k}} = \frac{\tilde{\varphi}_{\mathbf{k}}}{2\tilde{T}_{\parallel k}} = \frac{1}{\eta\tau} \left(1 - \eta k_{\perp}^2 - \sqrt{(1 - \eta k_{\perp}^2)^2 - \frac{\eta\tau\omega_d}{\omega_*}} \right). \quad (3.8)$$

Using (3.5) to parametrise all the unstable modes with an angle $0 \leq \theta \leq \pi$ like

$$k_{\perp}^2 = \frac{1}{\eta} \left(1 - \cos\theta \sqrt{\frac{\eta\tau\omega_d}{\omega_*}} \right), \quad (3.9)$$

one finds upon inserting this into the RHS of (3.8) and remembering that $\omega_{*0} < 0$ that it reduces to the simple expression

$$\frac{\tilde{\varphi}_{\mathbf{k}}}{\tilde{T}_{\perp \mathbf{k}}} = \frac{\tilde{\varphi}_{\mathbf{k}}}{2\tilde{T}_{\parallel \mathbf{k}}} = \sqrt{\frac{\omega_d}{\eta\tau\omega_*}} e^{ik_y\theta/|k_y|}. \quad (3.10)$$

Now since the radial heat flux is given by

$$Q = \frac{1}{L_x L_y} \int \hat{x} \cdot \mathbf{v}_{\mathbf{E}}(\tilde{T}_{\perp} + \tilde{T}_{\parallel}) dy dx = \sum_{\mathbf{k}} \text{Re} \left(ik_y \tilde{\varphi}_{\mathbf{k}}^* (\tilde{T}_{\perp \mathbf{k}} + \tilde{T}_{\parallel \mathbf{k}}) \right), \quad (3.11)$$

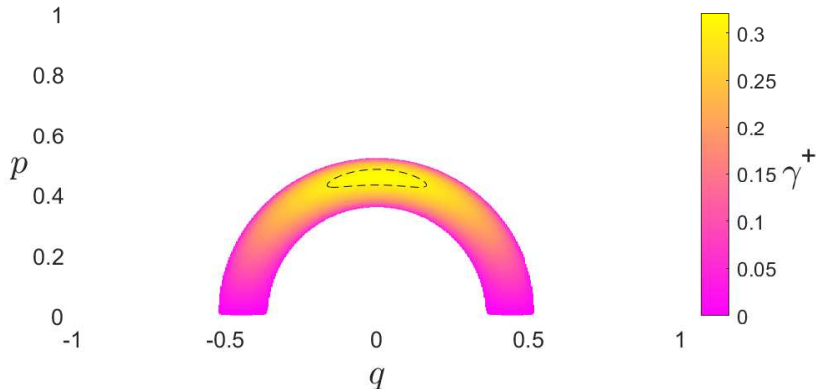


FIGURE 1. Primary drift wave growth rate $\gamma_{\mathbf{k}}^+$ for $(\omega_{d0}, \omega_{s0}, \tau, \eta) = (-0.1, -2, 0.5, 5)$ as a function of the radial and poloidal wavenumbers q and p respectively. The instability boundary for primary unstable modes, in the presence of that D for which this configuration constitutes the Dimits threshold, is also shown.

(3.10) implies that each mode provides a positive contribution to the total heat flux, since

$$\text{Re} \left(i k_y \tilde{\varphi}_{\mathbf{k}}^* (\tilde{T}_{\perp \mathbf{k}} + \tilde{T}_{\parallel \mathbf{k}}) \right) = 3 \sqrt{\frac{\omega_d}{\eta \tau \omega_*}} |\tilde{\varphi}_{\mathbf{k}}|^2 k_y \sin \left(\frac{k_y \theta}{|k_y|} \right) \geq 0. \quad (3.12)$$

Additionally, (3.10) makes it clear that the potential component of the mode decreases compared to its temperature as η increases. This linear result is in accordance with the intuitive picture that temperature fluctuations should grow in amplitude compared to the potential fluctuations as the temperature gradient is increased.

3.2. Secondary Instability

Within the primary-secondary-tertiary hierarchy, the secondary instability develops once the primary drift waves have grown sufficiently such that slight flow inhomogeneities begin to amplify through a shearing interaction to magnify small zonal perturbations. It is analytically best treated via a Galerkin truncation of (2.11)-(2.14) into the 4-mode system consisting of the most unstable single primary mode, its two sidebands, and a single zonal mode:

$$\mathbf{p} = (0, p), \quad \mathbf{r}^{\pm} = (\pm q, p), \quad \mathbf{q} = (q, 0). \quad (3.13)$$

The potential and temperature amplitudes of the primary mode are then fixed and taken to be much larger than other variables so that the linear terms of the sidebands can be ignored compared to the nonlinear interaction with the primary mode, which now becomes linearised. Then it is straightforward to obtain the secondary dispersion relation

$$\lambda^2 + 4p^2 q^2 \left| \tilde{T}_{\perp p} \right|^2 \left(\frac{2q^2}{\tau} - \text{Re} \left(\frac{\tilde{\varphi}_p}{\tilde{T}_{\perp p}} \right) \right) = 0. \quad (3.14)$$

Inserting the potential/temperature ratio of the unstable mode (3.8) into (3.14) is now natural since it is this mode which in the primary-secondary paradigm initiates the secondary instability, and this results in

$$\lambda^2 + \frac{4p^2 q^2 \left| \tilde{T}_{\perp p} \right|^2}{\eta \tau} \left(2\eta q^2 + \eta p^2 - 1 + \text{Re} \sqrt{(1 - \eta p^2)^2 - \frac{\eta \tau \omega_d}{\omega_*}} \right) = 0. \quad (3.15)$$

The last, stabilising term in (3.15) is similar to the opposite of the destabilising term of γ_k^+ in 3.2, but gives rise to a discontinuity instead of a bifurcation at

$$\eta p^2 = 1 \pm \sqrt{\frac{\eta \tau \omega_d}{\omega_*}}, \quad (3.16)$$

a feature which can clearly be seen in Figure 2 where the secondary growth rate is plotted. As p approaches the lower threshold from below, the radical in (3.15) approaches 0, causing λ to rapidly increase until its derivative with respect to p discontinuously flattens.

Now the absolute requirement on the zonal wavenumber in order for an unstable primary mode to be secondary unstable is established by equation (3.15) to be

$$q^2 < \frac{1 - \eta p^2}{2\eta}. \quad (3.17)$$

This means that modes with $p^2 > \eta$, and in particular the most unstable mode satisfying (3.3), are completely stable to the secondary instability and so can continue to grow unabated until another channel for zonal flow generation is established.

One might suspect that the of zonal flow would be initiated by those less unstable primary modes with smaller p which able to satisfy (3.17) once they have grown to a sufficient amplitude. However, in the simulations it is instead observed that, since the primary growth rate is rather sharply peaked around (3.3), these modes do not grow fast enough to be dynamically relevant at this stage. Instead, it seems that, since the small q -sidebands of the most unstable primary mode grow at nearly the same rate, it is their mutual sideband-sideband-interaction which jumpstarts the zonal growth. This is evidenced by the fact that the initial zonal growth rate remains mostly unchanged even when all modes but the most unstable primary mode and its sidebands are set to 0.

3.3. Local Tertiary Instability

Turning now to the final stage of the primary-secondary-tertiary hierarchy, once the zonal flow has grown enough to quench the drift waves the tertiary instability is that instability which allows the drift waves to reemerge from a zonally dominated state. In analysing this instability we will consider two separate limits, one localised and one de-localised (i.e. localised in k -space).

In the localised case, it is a well-known feature of tertiary modes that they localise to regions of zero zonal shear rate, $\partial_x^2 \bar{\varphi} = 0$ (Kobayashi & Rogers 2012; Kim *et al.* 2018, 2019). Therefore we should consider a poloidal band of modes ($k_y = p$) subject to a large amplitude zonal flow localised around such a point. In real x -space equations (2.11)-(2.14) then become

$$(\partial_t + ip\partial_x \bar{\varphi}) \tilde{T}_\perp - \frac{i\eta\omega_* \tilde{\varphi}}{2} = -D\tilde{T}_\perp \quad (3.18)$$

$$(\partial_t + ip\partial_x \bar{\varphi}) \tilde{T}_\parallel - \frac{i\eta\omega_* \tilde{\varphi}}{4} = -D\tilde{T}_\parallel \quad (3.19)$$

$$\begin{aligned} & \tau (\partial_t + ip\partial_x \bar{\varphi}) \tilde{\varphi} - i\omega_* (1 - \eta(p^2 - \partial_x^2)) \tilde{\varphi} \\ & + i \left(\frac{\omega_d}{4} + 2p\partial_x^3 \bar{\varphi} + 2p\partial_x^2 \bar{\varphi} \partial_x \right) \tilde{T}_\perp + i \frac{\omega_d}{2} \tilde{T}_\parallel = -D\tilde{\varphi}. \end{aligned} \quad (3.20)$$

so that if we consider a narrow region in which $\partial_x \bar{\varphi}$ and $\partial_x^3 \bar{\varphi}$ are approximately constant and allow ourselves to consider the mode to also be localised around the most unstable

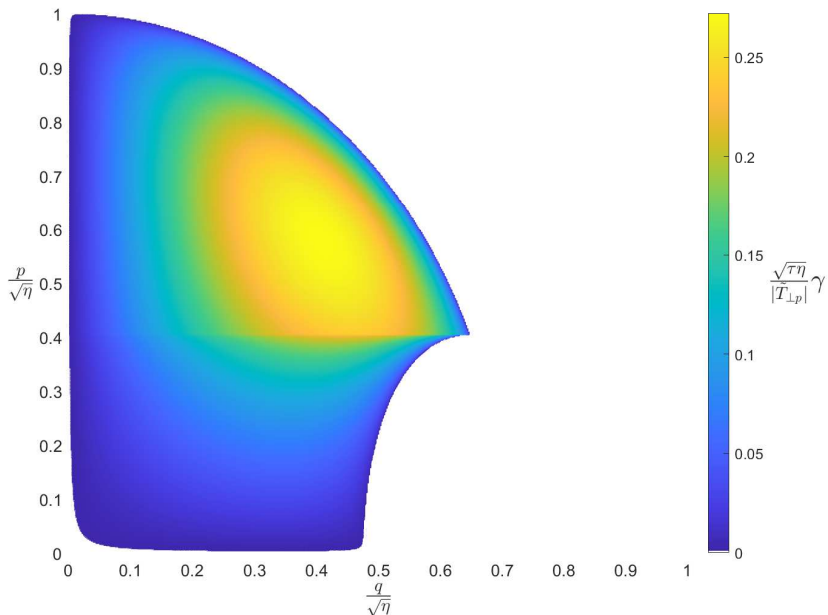


FIGURE 2. Secondary growth rate as a function of q and p for $\eta\tau\omega_d/\omega_* = 0.7$. The bifurcation at (3.16) is clearly visible.

primary mode with $k_x \approx 0$, we arrive at the local tertiary dispersion relation

$$\lambda^\pm = -D + i \left(\frac{\omega_* - \eta\omega_*(p^2)}{2\tau} - p\partial_x\bar{\varphi} \right) \pm \frac{\omega_*}{2\tau} \sqrt{(1 - \eta(p^2))^2 - \frac{\eta\tau}{\omega_*}(\omega_d + 8p\partial_x^3\bar{\varphi})}. \quad (3.21)$$

As is easily seen, this expression is precisely the linear dispersion of the primary mode (3.2) Doppler shifted by $p\partial_x\bar{\varphi}$ and with a zonal shear modified magnetic curvature. We note that the real part of this expression vanishes when the driving gradients are removed, meaning that no tertiary instability exists at all in their absence. We are thus dealing here with only a modified primary, extracting energy from the background gradients, rather than from the zonal flow like the KH instability (see Zhu *et al.* 2020a). To recover the latter the inclusion of zonal temperature perturbations is required (Rogers *et al.* 2000; Ivanov *et al.* 2020), but since this instability has been shown to be mostly irrelevant in the Dimits regime by Rath *et al.* (2018) there is no urgent need to do so.

Returning to the specific expression (3.21), we see that the tertiary instability is asymmetric with respect to zonal flow velocity minima, $\partial_x^3\bar{\varphi} > 0$, and maxima $\partial_x^3\bar{\varphi} < 0$; the former is destabilising while the latter is stabilising. This asymmetry matches gyrokinetic observations that zonal flow shear minima are significantly more prone to turbulent transport (McMillan *et al.* 2011), and has already been noted in previous tertiary instability studies of simple systems (see e.g. Zhu *et al.* 2020a). Though the presence of zonal temperature perturbations considerably complicates the picture in the closely related system of Ivanov *et al.* (2020), for us the tertiary prediction (3.21) matches simulations well and, as we will see in Section 4, the turbulence is consistently localised around the points at which $\partial_x^2\bar{\varphi} = 0$ and $\partial_x^3\bar{\varphi} > 0$.

3.4. 4-Mode Tertiary Instability

We now proceed to study the tertiary instability of a sinusoidal profile corresponding to the mode $\overline{\varphi}_q$. In order to gain further insight we employ the same 4-mode (4M) Galerkin truncation (3.13) for simplification as we did for the secondary instability, even though it in general it is less justifiable here. Naturally with so few modes this analysis will fail to capture any intricate localisation effects, but we will nevertheless be able to discern some important features of the tertiary instability. After all, (3.21) employed strong approximations (e.g. fully neglecting k -space coupling), which may in general not be satisfied.

Assuming without loss of generality that $\overline{\varphi}_q$ is real (all results herein will only depend upon its magnitude), i.e.

$$\overline{\varphi} = 2\overline{\varphi}_q \cos qx, \quad (3.22)$$

the 4M tertiary dispersion relation can after some algebra, analogous to that of Section 3.2, be expressed as

$$\mathcal{D}_{Pr}\mathcal{D}_T\mathcal{D}_{MP} = 0. \quad (3.23)$$

This factorised form of the dispersion relation delineates the different linear solutions, corresponding to zeros of each of the three factors. The equation $\mathcal{D}_{Pr} = 0$ is the unmodified primary dispersion relation of the sidebands r with solutions (3.1) and (3.2), corresponding to a solution of (2.11)-(2.14) where the primary mode is absent (i.e. the \mathbf{p} -mode is 0) and the sidebands are of equal amplitude. Next

$$\mathcal{D}_T = (\lambda + D_p)(\lambda + D_r) + 2p^2q^2\overline{\varphi}_q^2 = 0 \quad (3.24)$$

is the dispersion relation of two stable pure temperature modes as affected by the zonal flow, and finally

$$\mathcal{D}_{MP} = (\lambda - \lambda_p^+)(\lambda - \lambda_p^-)(\lambda - \lambda_r^+)(\lambda - \lambda_r^-) + 4p^4q^4\overline{\varphi}_q^4 + Ap^2q^2\overline{\varphi}_q^2 = 0, \quad (3.25)$$

where

$$\begin{aligned} A(\lambda) = & 4(\lambda + D_p)(\lambda + D_r) + \frac{\eta\omega_*\omega_d}{\tau} - 2\frac{\omega_*^2}{\tau^2}(1 - \eta p^2)^2 \\ & + 2i\frac{\omega_*}{\tau}((\eta p^2 - 1)(2\lambda + D_p + D_r) - \eta q^2(\lambda + D_r)), \end{aligned} \quad (3.26)$$

is the dispersion relation of the 4M zonal flow modified primary mode, containing the tertiary mode.

Let us consider the dispersion relation of the modified primary in the large zonal flow limit. Expanding (3.25) in orders of $\overline{\varphi}_q$ like

$$\lambda = \lambda_1 + \lambda_{1/2} + O(1), \quad (3.27)$$

we find, after collecting terms up to to order $\sqrt{\overline{\varphi}_q}$ and using (3.2), that (3.25) can be reduced to

$$(\lambda^2 + 2p^2q^2\overline{\varphi}_q^2)^2 + B\lambda^3 + (2B - 4i\frac{\omega_*}{\tau}\eta q^2)p^2q^2\overline{\varphi}_q^2\lambda = 0, \quad (3.28)$$

where

$$B = -(\lambda_p^+ + \lambda_p^- + \lambda_r^+ + \lambda_r^-) = 2(D_p + D_r) + \frac{i\omega_*}{\tau}(\eta(q^2 + 2p^2) - 2). \quad (3.29)$$

At leading $O(\overline{\varphi}_q^2)$ -order (3.28) yields the purely oscillating solutions

$$\lambda_1 = \pm\sqrt{2ipq\overline{\varphi}_q}, \quad (3.30)$$

similar to the modes of (3.24). In order to find the real part of these modes we then

have to proceed to order $O(\overline{\varphi}_q)$ since the $O(\overline{\varphi}_q^{3/2})$ -part identically vanishes. At that order (3.28) yields

$$-4\lambda_{1/2}^2\lambda_1^2 - 4i\frac{\omega_*}{\tau}\eta q^2 p^2 q^2 \overline{\varphi}_q^2 \lambda_1, \quad (3.31)$$

and thus

$$\lambda_{1/2} = \pm \sqrt{\pm \frac{\eta\omega_* q^2}{\sqrt{2}\tau} \sqrt{pq\overline{\varphi}_q}}. \quad (3.32)$$

Combining these results, in the large $\overline{\varphi}_q$ -limit we therefore have the four solutions

$$\lambda_{p,r}^\pm = \sqrt{2}ipq\overline{\varphi}_q \pm \sqrt{\frac{\eta\omega_* q^2}{\sqrt{2}\tau} \sqrt{pq\overline{\varphi}_q}}, \quad (3.33)$$

$$\lambda_{p,r}^{s\pm} = -\sqrt{2}ipq\overline{\varphi}_q \pm i\sqrt{\frac{\eta\omega_* q^2}{\sqrt{2}\tau} \sqrt{pq\overline{\varphi}_q}}, \quad (3.34)$$

of which only the first is unstable. Note that we henceforth will use the notation $\lambda_{p,r}^\pm$ to refer to the most unstable and most stable coupled modes, regardless of whether $\overline{\varphi}_q$ is large or not.

Converting the solutions corresponding to (3.33) from k -space to real space using the zonal profile (3.22) we find that they take the form

$$\tilde{\varphi} = \left(1 \pm \sqrt{2} \sin qx\right) \operatorname{Re} \left(e^{ipy + \lambda_{p,r}^\pm t} \right). \quad (3.35)$$

It is apparent that the x -envelope, being given by the first factor, predominantly localises the unstable mode around minima of the zonal flow velocity and the stable mode around maxima, entirely in accordance with the picture that these points are tertiary (de-)stabilising as outlined in Section 3.3. Furthermore it is seen that, despite not being sufficiently localised for the treatment of Section 3.3 to be justified, this result nevertheless agrees with the large $\overline{\varphi}$ -limit of (3.21) up to numerical constants.

Now turning to the opposite small $\overline{\varphi}_q$ -limit, we are interested in how the unstable primary mode is modified by the presence of a small zonal flow. Taylor expanding (3.25) around $\lambda = \lambda_p^+$ one straightforwardly obtains the solution

$$\lambda = \lambda_p^+ - Cp^2 q^2 \overline{\varphi}_q^2 \quad (3.36)$$

where

$$C = \frac{A(\lambda_p^+)(\lambda_p^+ - \lambda_r^+)^\dagger(\lambda_p^+ - \lambda_r^-)^\dagger}{(\lambda_p^+ - \lambda_p^-)|(\lambda_p^+ - \lambda_r^+)(\lambda_p^+ - \lambda_r^-)|^2}. \quad (3.37)$$

Let us now employ a subsidiary ordering in q to see how $\operatorname{Re}(C)$ behaves in the two limits $q^2 \ll 1$ (keeping $q^2 \gg \overline{\varphi}_q^2$) and $q^2 \gg 1$ (keeping $q^2 \overline{\varphi}_q^2 \ll 1$) to see whether the growth rate of the most unstable mode is initially stabilised or destabilised by the presence of zonal flows at these scales. Because it is apparent that the denominator of (3.37) is positive and because the numerator of C becomes

$$-2\frac{\omega_*^2 \eta^2 q^4}{\tau^2} (|\lambda_p^+|^2 + D_r \gamma_p^+), \quad (3.38)$$

for large q -values, it is apparent that $\operatorname{Re}(C)$ is negative for small scale zonal flows which therefore are destabilising already at small amplitude. As $\overline{\varphi}_q$ is further increased we furthermore know that it transitions into the unstable mode (3.33), and so we can conclude that small scale zonal flows are always destabilising. In fact it is numerically

found that the transition to instability with increasing q occurs much before this limit, already as $q \sim p$ as can be seen in Figure 3. Note that this point is still much below that where the KH-like $(qp\bar{\varphi}_q)^\alpha$ -scaling of (3.33) develops, and thus the mode is still ostensibly "more primary" in character.

If q on the other hand is small, the numerator of C becomes

$$16\gamma_p^{+2} \left(i\frac{\omega_*}{2\tau} - \frac{\omega_*^2(1-\eta p^2)}{4\tau^2\gamma_p^+} \right) \eta q^2. \quad (3.39)$$

This has a positive real part for those modes with $\eta p^2 > 1$, including the most unstable primary mode satisfying (3.3), and so small scales zonal flows are initially stabilising for these modes. It should be noted that the fact that this result goes in the opposite direction for modes of smaller p does not mean that the zonal flow initially destabilises large scale drift waves. As can be seen from the linear growth rate (3.2), at these scales the small q sidebands are in fact more unstable than their primary mode. Thus upon repeating the calculation above, but instead expanding around $\lambda = \lambda_r^+$, one finds precisely the opposite stabilisation effect on the sidebands. These results can be summarised by the observation that, at small zonal amplitude, the tertiary mode constitutes a sort of average of its constituent primary modes, with the final rate of growth (or decay) situated in between.

With the asymptotic behaviour of (3.33) and (3.36) in hand, it is clear that the initial stabilisation (3.36) of small amplitude zonal flows must reverse as the amplitude is increased, and there necessarily exists some zonal flow amplitude which is most stable. Precisely this can be seen in Figure 3, where the most unstable 4M tertiary growth rate $\gamma_{p,r}^+$ for the example system $(\omega_{d0}, \omega_{s0}, \tau, \eta, D) = (-0.8, -1.02, 1, 1.8, 0.5)$ with linear instability threshold $\eta^0 = 1.64$ (which will be the focus of the remainder of this paper), is plotted. In accordance with (3.38) and (3.39), as $\bar{\varphi}_q$ begins to be increased the tertiary mode initially stabilises for $q \lesssim p$, while destabilising for q beyond.

3.5. Role of the Tertiary Instability for the Dimits transition

Extrapolating the consequences of the findings above to the dynamics of the zonally dominated states typical of the Dimits regime, some conclusions can be drawn. If conditions of the zonal profile are not ideal, it will fail to suppress the tertiary instability, which will grow in amplitude to eventually affect the zonal profile. While such conditions prevail, the zonal profile will evolve through different configurations in a process we will refer to as *zonal profile cycling*. In this process, energy will continue to be injected into the drift waves at a faster rate for more tertiary unstable zonal profiles. Thus the profile should be observed with higher probability in a state of low tertiary growth. Indeed, it is expected that a state of absolute tertiary stability could be sustained indefinitely. In conclusion we argue that the tertiary instability therefore preferentially selects a set of zonal profiles which will predominantly appear as the system evolves.

Because the zonal flows by construction are linearly undamped, a tertiary stable zonal profile can emerge that sustains the system in a state of suppressed turbulence, so long as the decaying residual drift wave activity, in turn, does not affect it too much. We will refer to such profiles as *robustly stable*. Now, from the 4M-result above, we can extrapolate that the tertiary instability for our system exhibits only a finite ability to be stabilised. Naturally this means that as the driving gradient η is increased the number of robustly stable zonal profiles should decrease. Eventually, at some point none remain and turbulence and transport arises. If this point indeed corresponds to the Dimits transition,

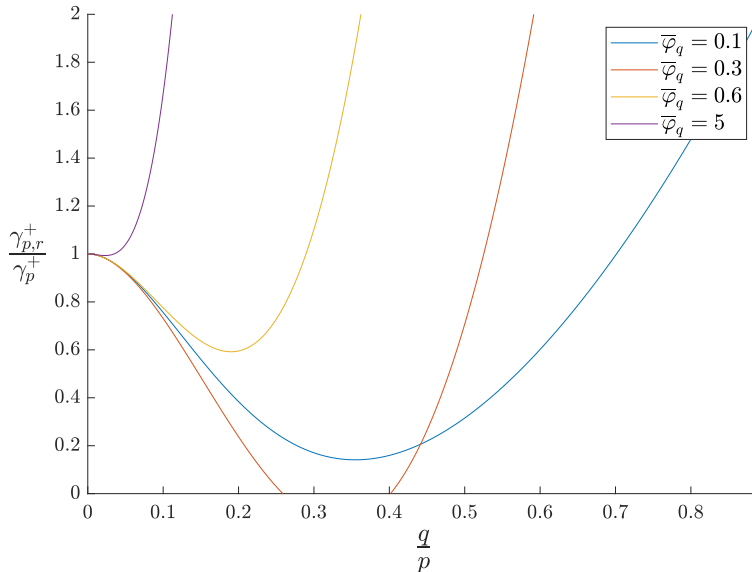


FIGURE 3. 4-mode tertiary growth rate $\gamma_{p,r}^+$, normalised by the unmodified primary growth rate γ_p^+ , as a function of the zonal wavenumber q for $\varphi = 0.1, 0.3$, and 0.6 respectively for $(\omega_{d0}, \omega_{*0}, \tau, \eta, D) = (-0.8, -1.02, 1, 1.8, 0.5)$.

then the only the relevant features needed to explain the Dimits shift should be the tertiary instability and the ability of the zonal flows to cycle through stabilising profiles.

Of course it is possible that even in the absence of collisional zonal damping a stable zonal state cannot be attained. Another possibility is that, above the tertiary instability threshold, some nonlinear mechanism continues to reduce the transport, making the Dimits threshold of appreciable transport not coincide with the tertiary threshold. An example of such a feature, already observed and explored in other systems, would be e.g. the ferdinons of (Ivanov *et al.* 2020). For our system however, this does not seem to be the case, and, as we will see, the tertiary instability alone seems sufficient to explain the Dimits shift. That is, below a certain point $\eta = \eta^n$, tertiary stable zonal profiles are always able to form and completely quench transport, while above it they cease to manifest and the time-averaged transport levels rapidly increase with η .

In conclusion, it should be noted that precisely what profiles are robust is a delicate and highly nontrivial question, which nevertheless ultimately decides when the Dimits transition occurs. Thus the tertiary instability should not enter Dimits shift picture via so simple a rule as “the Dimits regime should end when the zonal amplitude becomes too large” (Rogers *et al.* 2000; Rath *et al.* 2018), nor “the Dimits regime should end when the zonal amplitude becomes too small” (Zhu *et al.* 2020a). Though the latter may hold when collisional damping limits the zonal amplitude, in general it is the much more nebulous question of “can a robust zonal profile be reached and sustained during the subsequent transient period of decay” which must be answered.

4. Nonlinear simulation results

In order to thoroughly investigate the strongly driven system, it was first simulated pseudospectrally for several configurations on a square grid using a sixth order Runge-Kutta-Fehlberg method including 512×256 modes with $0 < k_x, k_y \leq 5p_m$ and with

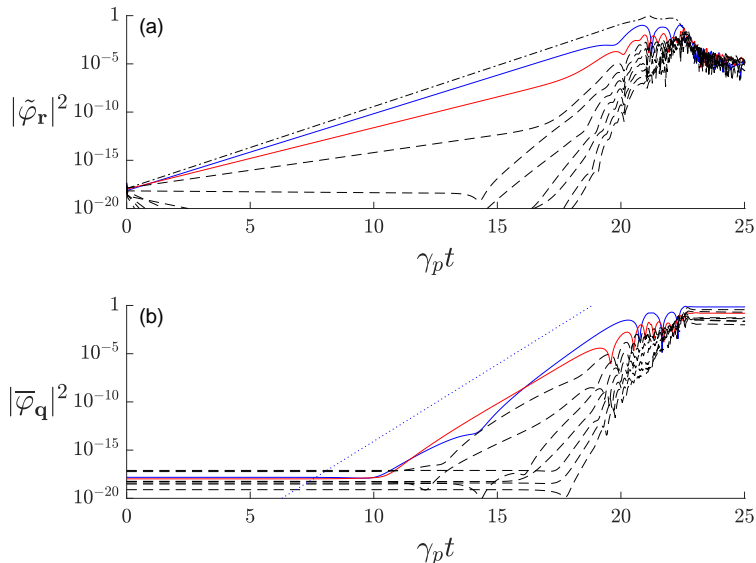


FIGURE 4. (a) Drift wave and (b) zonal mode amplitudes during the initial growth phase. The blue line corresponds to the lowest q (longest wavelength) fundamental mode q_{\min} , the red line to the second harmonic $2q_{\min}$, and other modes are denoted by black dashed lines. After an initial linear phase, the sideband-sideband-interaction of $\tilde{\varphi}_{(q_{\min},p)}$ excites the first and second zonal fundamentals, which thus grow at a rate proportional to $|\tilde{\varphi}_{(q_{\min},p)}|^2$, which is plotted with a dotted line for comparison. Modes of higher and higher q are then excited one by one, until the zonal flows reach a magnitude comparable to the drift waves, which are then suppressed.

dealiasing using the 3/2-rule. Sensitivity scans with regards to the number of modes and the minimum wavenumbers found this selection to be well beyond what was necessary for relevant results to convergence, so long as the most unstable drift wave p_m was included.

The nonlinear simulations usually employed a k -independent D , to be discussed in Section 5.1, and were initiated with small Gaussian noise of (normalised) energy density 10^{-8} . As can be seen in Figure 4, the expected behaviour is then observed where primary modes emerge until they are strong enough to nonlinearly engage the zonal modes. In accordance with the secondary mode analysis of 3.2, sideband-sideband interactions here play a vital role for initial zonal mode growth to occur, and so necessarily the second zonal mode q_{\min} -fundamental is primarily engaged. During this stage, only the largest scale zonal modes grow appreciably, but once they reach sufficient amplitude, nonlinear interactions quickly shuffle energy from the unstable modes to higher and higher q -sidebands. These, in turn, engage higher q zonal modes to affect the primary growth, and the growth phase ceases. This typically occurs when both the drift wave and zonal flow energy densities reach a comparable magnitude of around 1.

It is important to note that, as a consequence of there being no direct coupling between drift waves of differing poloidal wavenumber, the system typically stratifies into separate p -layers only interacting with each other via their influence on the zonal flow. In the Dimits regime, where necessarily $D \sim \gamma_p^+$, only those few modes with p around p_m , satisfying (3.3), are linearly unstable. Consequently, the layer corresponding to the dominant primary mode becomes solely dynamically important. Though the zonal profile could excite other bands through the tertiary instability, since the primary band is the most tertiary unstable this is not borne out in practice. More layers become important

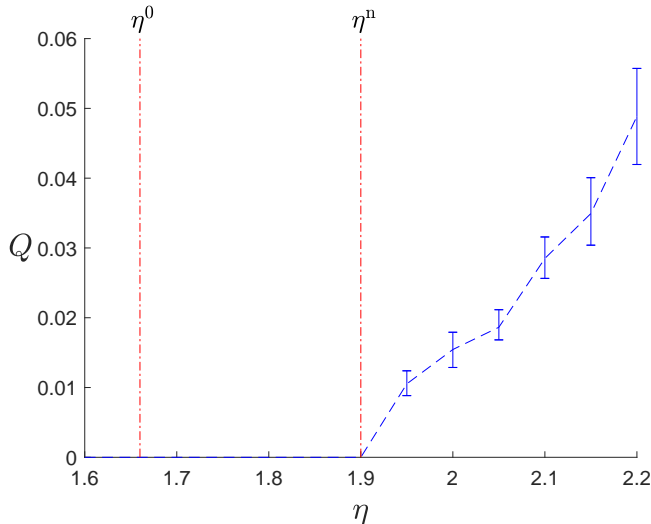


FIGURE 5. Long time-averaged heat flux, given by (3.11), as a function of η . The linear instability threshold occurs at $\eta^0 \approx 1.66$, yet finite heat flux only commences beyond $\eta^n \approx 1.9$, constituting a clear Dimits shift. Between these points, the system relaxes to completely stable purely zonal states.

only once they become primary unstable at larger η -values, occurring above the point at which the transition to continuous transport occurs.

Now, initial saturation amplitudes of both zonal and drift waves exhibit a very slight dependence on the initialisation amplitude. This is because differing primary/sideband growth rates causes there to be more or less initial energy to distribute, depending on the amount of time the primary mode has had to grow before the sidebands trigger zonal growth. Nevertheless, in the Dimits regime the zonal amplitude usually quickly returns to a system-parameter-dependant typical amplitude, like the tertiary analysis of 3.4 suggests. Once there, a staircase-like state, similar to those observed by Dif-Pradalier *et al.* (2010) or Kobayashi & Rogers (2012), quickly develops, which can then efficiently suppress drift wave amplitudes, typically on the order of 2 magnitudes (but occasionally much more). All that remains then are the localised tertiary modes which will eventually die if stable or grow back if unstable. Observing the heat flux after a long time has passed, like in Figure 5, the presence of Dimits shift is thus revealed, since stable states only exist close to the linear threshold η^0 .

4.1. Drift Wave Bursts

As can be seen Figure 6, when the instability parameter η is increased away from the linear threshold η^0 while other parameters are kept the same, the initial zonal profiles attained are commonly completely tertiary stable. However as η is further increased this usually ceases to be the case, since the primary/sideband coupling then fails to remain strong enough for the primary mode to decay together with the damped sidebands. Consequently, a spreading turbulence burst destroys the initial zonal staircase, cycling through zonal profiles until another stable state is reached. The rapidity by which such bursts occur, and the time until a stable zonal profile is attained, both rapidly increase with η , unless the cycling by happenstance quickly produces a stable state. At even larger η -values, no stable state is ever attained. Furthermore, the typical burst amplitude is also reduced as a result of less efficient drift wave quenching.

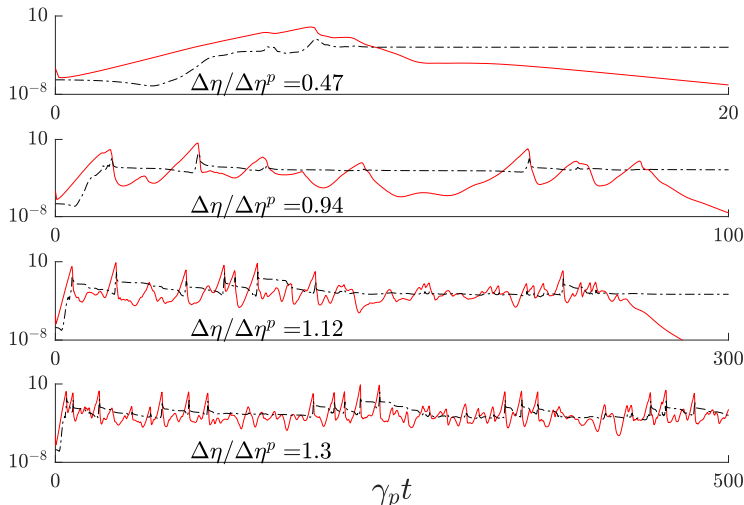


FIGURE 6. Time evolution of the zonal (black dashed) and nonzonal (red) energy densities $E_{\bar{\varphi}}$ and E_{φ} for some configurations of increasing instability $\Delta\eta = \eta - \eta^0$ where η^0 is the linear instability threshold and $\Delta\eta^p$ is the predicted Dimits transition as introduced in Section 5. As the system becomes more unstable it is observed to take longer arrive at a completely stable zonal state, while simultaneously exhibiting more rapid bursty behaviour.

Note that this entire burst pattern is, on the surface, similar to the zonal/drift predator-prey interactions commonly observed in many systems as a result of zonal damping (see e.g. Malkov *et al.* 2001; Kobayashi & Rogers 2012). However, it differs fundamentally in that the turbulent bursts are not typically accompanied by large zonal amplitude swings. Instead, it traces its origin to tertiary mode localisation.

To see how this is the case, some snapshots of a typical burst are displayed in Figure 7. A zonal staircase is observed which, in accordance with (3.21), predominantly exhibits tertiary modes localised at the points where the conditions $\partial_x^2\bar{\varphi} = 0$, and $\partial_x^3\bar{\varphi} > 0$ are satisfied. Eventually that at $x \approx 32$ grows enough to affect the zonal profile at this point, resulting in a central flattening of the zonal amplitude. While the zonal shearing rate $\partial_x^2\bar{\varphi}$ remains 0 in the process, $\partial_x^3\bar{\varphi}$ is reduced, except for at the boundary of the full mode, causing a central tertiary instability reduction. The tertiary mode now becomes more more unstable at its boundary, where the condition $\partial_x^3\bar{\varphi} > 0$ is still maintained. As a result, the zonal flattening continues and the tertiary mode broadens behind a propagating zonal front, eventually encompassing much of the domain and destroying the zonal staircase.

After a period of zonal profile cycling, a zonal staircase is eventually reestablished, which again quenches the drift waves down to the original amplitude. The tertiary instability is now however localised at different points, where seeded drift waves can eventually repeat the process. However, these points were initially tertiary stable, and so it takes a long time for a localised mode to fully develop. This explains the large transport level swings at marginally unstable η -values observed in Figure 6.

As a final remark it is worth noting that during the entire burst process, the box averaged zonal shear magnitude $|\partial_x^2\bar{\varphi}|$ remains comparable to the primary growth rate γ^+ . This is a typical result also obtained in previous investigations of zonally dominated

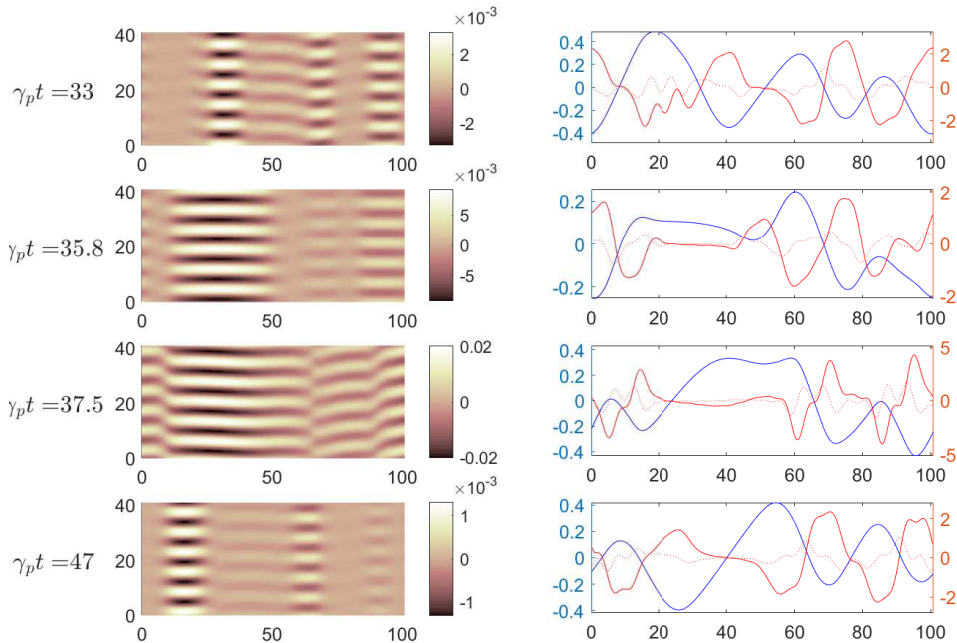


FIGURE 7. Snapshots of driftwaves, the zonal profile φ_x (blue), zonal flow shear $\partial_x^2 \varphi_x$ (red), and its derivative $\partial_x^3 \varphi_x$ (dotted red). These depict a turbulent burst originating as an unstable tertiary mode at $x \approx 32$ where $\partial_x^2 \varphi_x = 0$ and $\partial_x^3 \varphi_x > 0$ at $\gamma_p t = 33$, broadening and growing in amplitude between two tertiary unstable propagating zonal fronts at $\gamma_p t = 35.8$ until the driftwaves encompass the whole volume at $\gamma_p t = 37.5$, rapidly modifying the zonal profile until a new zonally dominated state can be reinstated at $\gamma_p t = 47$, but which exhibits seeded tertiary modes at $x \approx 17$ and $x \approx 64$ which will eventually repeat this process.

states (Waltz *et al.* 1998; Kinsey *et al.* 2005; Kobayashi & Rogers 2012) known as the quench rule.

5. Reduced mode Dimits shift estimate

Having identified the importance of the tertiary instability for the Dimits transition in Sections 3.3, 3.4, and 4, we now turn our attention to the problem of attempting to predict the size of the Dimits shift using tertiary instability analysis. For the system under consideration it is clearly necessary that there exists tertiary stable zonal profiles for the system to be located within the Dimits regime. This has been exploited before by Zhu *et al.* (2020*a,b*) in other systems where full stability characterises the Dimits regime to match the Dimits shift threshold to a tertiary transition. However this matching could only be done in hindsight by tuning a representative zonal curvature value by hand, and did thus not constitute a prediction.

To predict the Dimits shift the major problem one encounters is, as we outlined in Section 3.5, the full multitude of possible zonal profiles, and accounting for how these can be generated through nonlinear interactions with the drift waves. Some profiles may fail to form nonlinearly, while others fail to be robustly stable enough to persist while the residual drift waves decay. Thus it may not be sufficient that a tertiary stable zonal profile

exists for the system to be in the Dimits regime. Thoroughly accounting for this seems a herculean task and instead some major simplifying assumptions have to be employed.

An example of a simple method doing just that is the heuristic prediction of St-Onge (2017), which relies on the same tertiary 4-mode Galerkin truncation as (3.13) in lieu of accounting for the complex interplay of the many modes constituting the full zonal flow profile. In a modified Terry-Horton system it was postulated that a typical mode could be approximated by that maximally coupling the tertiary 4M to satisfy the condition $\lambda_{\mathbf{p},\mathbf{r}}^+ = \lambda_{\mathbf{p},\mathbf{r}}^-$. Approximating the coupling of the primary mode to its sidebands through the 4M-interaction alone, and assuming that it is the most unstable primary mode that determines when the Dimits regime ends, the Dimits transition was then taken to occur when this cluster of maximally coupled modes became unstable.

St-Onge (2017) found this prediction to be in excellent agreement with the observed Dimits transition. However the sensitivity of this transition to numerical dissipation, the small transport levels immediately beyond this point, and the slow evolution made it somewhat difficult to definitively classify a state as stable or turbulent close to this threshold in subsequent reproductions of this system by Zhu *et al.* (2020b). On the other hand, for our purposes the major flaw of this prediction is the fact that, with the inclusion of 3 modes for each \mathbf{k} , there ceases to form anything resembling maximally coupled modes. Nevertheless, because of the simplicity of such a scheme we now look for a similar zonal profile reduction to arrive at a reduced mode prediction.

The first key feature of the present system when attempting to arrive at a simplified prediction is the aforementioned stratification observed in the nonlinear simulations. As mentioned, it is the poloidal band corresponding to the most unstable primary mode \mathbf{p} which goes tertiary unstable first, and thus solely determines when the Dimits regime ends. Secondly we recall the result of Section 3.5 that the tertiary instability frequently acts in such a way as to push the zonal amplitude $\overline{\varphi}_q$ towards its most stabilising value. At least as long as the 4M-interaction is dominant, the the zonal profile should therefore repeatedly evolve into a state similar to this one.

For the final piece of the puzzle a much more reductive simplification is employed which relegates this method firmly into being an estimate. We choose to approximate a typical full zonal profile with a single mode, with wavelength q , which is the most tertiary stabilising. Of course any real profile will include many more modes of varying amplitude. Nevertheless, some of these will act to destabilise and some to stabilise the tertiary modes, and so we assume that their cumulative effect can be approximated by a representative mode. Indeed the surprising qualitative similarity between the 4M tertiary growth rate in the high $\overline{\varphi}$ -limit (3.33) and the local tertiary (3.21) hints that this approximation may be less far-fetched than it seems.

Combining these pieces, we conclude that the Dimits transition should occur at around that point $\eta^{\mathbf{p}}$ where our single zonal mode ceases to be able to stabilise the most unstable primary mode, leaving no robustly stable zonal state attainable. Thus we can express our Dimits shift prediction $\Delta\eta^{\mathbf{p}}$ as

$$\Delta\eta^{\mathbf{p}} = \eta^{\mathbf{p}} - \eta^0, \quad (5.1)$$

where $\eta^{\mathbf{p}}$ is the solution to the constrained optimisation problem

$$\frac{\partial\gamma_{\mathbf{p}}^+}{\partial p} = 0, \quad (5.2)$$

$$\frac{\partial\gamma_{\mathbf{p},\mathbf{r}}^+}{\partial|\overline{\varphi}_q|} = 0, \quad (5.3)$$

$$\frac{\partial \gamma_{p,r}^+}{\partial q} = 0, \quad (5.4)$$

$$\gamma_{p,r}^+(\eta^{\text{P}}) = 0. \quad (5.5)$$

In Figure 8 this method can be seen in practice for the configuration of Section 4. Though we again stress that (5.1) is clearly a nonrigorous estimate of the Dimits transition, the broader accuracy of which has to be confirmed by comparison with nonlinear simulations we will perform in Section 5.1, this predicted Dimits transition at $\eta^{\text{P}} = 1.86$, corresponding to a Dimits shift of $\Delta\eta \approx 0.23$, is indeed close to the point $\eta^{\text{P}} \approx 1.9$ of Figure 5 where the drift waves observed in nonlinear simulations fail to vanish.

Now, in principle it should be possible to apply the estimation method as just outlined to other systems, up to and including gyrokinetics, so long as one is mindful of what zonal profiles are typically observed and whether some slight modification is necessary to account for these. However, it can only be expected to be useful so long as collisional damping is low enough for the Dimits regime to be characterised by sufficiently stable zonal states, so that the Dimits transition coincides with the point of tertiary destabilisation. Should this not be the case, some other method would have to be employed such as e.g. that of Ivanov *et al.* (2020), asymptotically accurate in the highly collisional limit, which investigates whether the effect of the turbulence upon the zonal flow either counteracts or reinforces its collisional dissipation.

5.1. Comparison of Prediction and Nonlinear Results

The question now is to what extent the prediction as just outlined in Section 5 is generally accurate. To investigate this question we are greatly aided by the observed poloidal stratification and how the dominant primary band is the most tertiary unstable. This means that we can restrict ourselves to only include zonal modes and the most unstable poloidal band in nonlinear simulations, which constitutes a tremendous speedup enabling us to investigate a very wide range of different configurations. This reduction was found to have no appreciable effect on the observed Dimits shift for any of the many disparate test cases, and seems to be uniformly valid for this investigation.

The specific way in which the Dimits shift for a configuration with a given $(\omega_d, \omega_*, \tau, \eta^0)$ was determined can be described as follows. A set of simulations with increasing η were performed and were allowed to run continuously until a fully stabilising profile was obtained and all drift-wave amplitudes died down below their original values. If this had not occurred within the time $t_{\text{end}} = 3000\gamma^{-1}$, the simulation was stopped, and the Dimits transition taken to be the final η where a stable state arose.

Across thousands of simulations and nearly a hundred configurations, it only happened a handful of times that a simulation with a higher η reached stability while one below it failed to do so, and in the few cases for which this occurred all were located right at the Dimits threshold. As outlined in Section 3.5, this is because the space of robustly stable zonal configurations rapidly shrinks to 0 at the true Dimits threshold η^{Di} , beyond which no stable states exist. Thus, although it occasionally happens that a stable profile is quickly obtained, the average time t_{avg} to attain one of these stable states in nonlinear simulations diverges at η^{Di} ,

$$\lim_{\eta \rightarrow \eta^{\text{Di}}} t_{\text{avg}} = \infty. \quad (5.6)$$

Therefore the observed Dimits transition η^{n} , obtained in nonlinear simulations, typically varies very little with respect to t_{end} once it is sufficiently large,

$$\lim_{t_{\text{end}} \rightarrow \infty} \frac{\partial \eta^{\text{n}}}{\partial t_{\text{end}}} = 0. \quad (5.7)$$

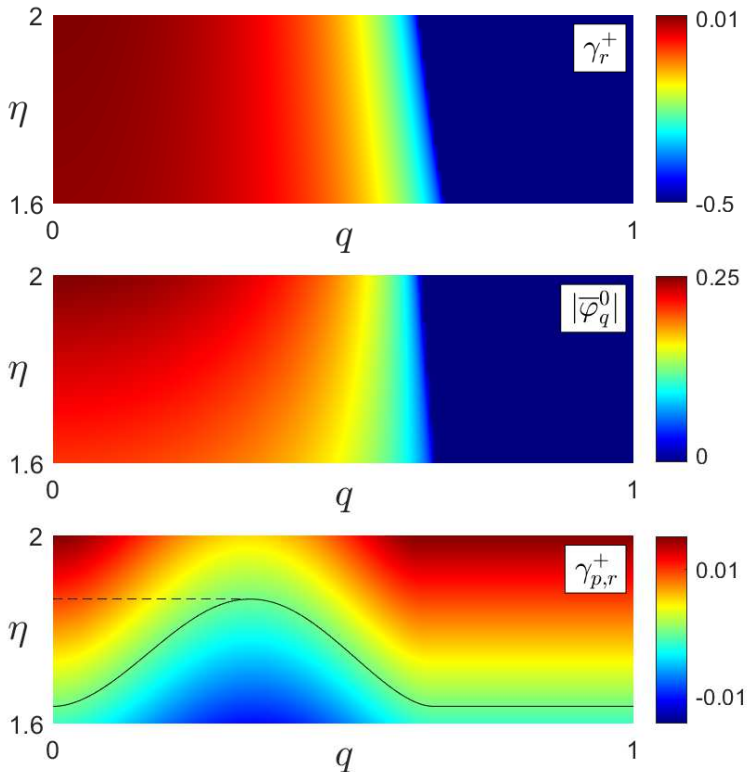


FIGURE 8. The primary instability growth rate γ_r , the most stabilising zonal amplitude $\overline{\varphi}_q^0$ satisfying (5.3), and its 4M-tertiary growth rate $\gamma_{p,r}^+$ as a function of η and q . The resulting 4M-tertiary Dimits prediction η^p is indicated by a dashed line, constituting a Dimits shift $\Delta\eta = \eta^p - \eta^0$ of ~ 0.23 .

With these observations we feel justified in claiming that this method of determining the Dimits shift is robust for our system.

A comparison of the the predicted Dimits shift $\Delta\eta^p$ and the nonlinearly obtained Dimits shift $\Delta\eta^n$ for configurations within the wide range given by $\omega_{d0} \in [-10, -10^{-5}]$, $(\omega_{*0}, \tau) \in [-10, -10^{-2}]$, $\eta^0 \in [10^{-0.5}, 10^{2.5}]$ can be seen in Figure 9. The prediction is seen to generally underpredict the Dimits shift by about 15% barring a few outliers varying by some 10%. Nevertheless this is a favourable result because of how very consistent it remains across such a wide range of different configurations, while ultimately being so simple. Indeed no trend for the deviation with respect to any parameter can be discerned.

What we have been investigating in this paper has been for the case of a flat (with respect to k_y) dissipation D . This has some physical justification in that a rigorous linear analysis of the full kinetic mode reveals, beyond the normal mode whose Landau damping can be approximated as viscous dissipation, the presence of an algebraically decaying continuum mode. In the marginally stable regime of interest the continuum modes of the sidebands should thus be dominant, since they decay much more slowly (Sugama 1999; Mishchenko *et al.* 2018). Unfortunately is very hard to accurately reproduce the behaviour of these modes within a spectral fluid model in a non-exotic way (Sugama

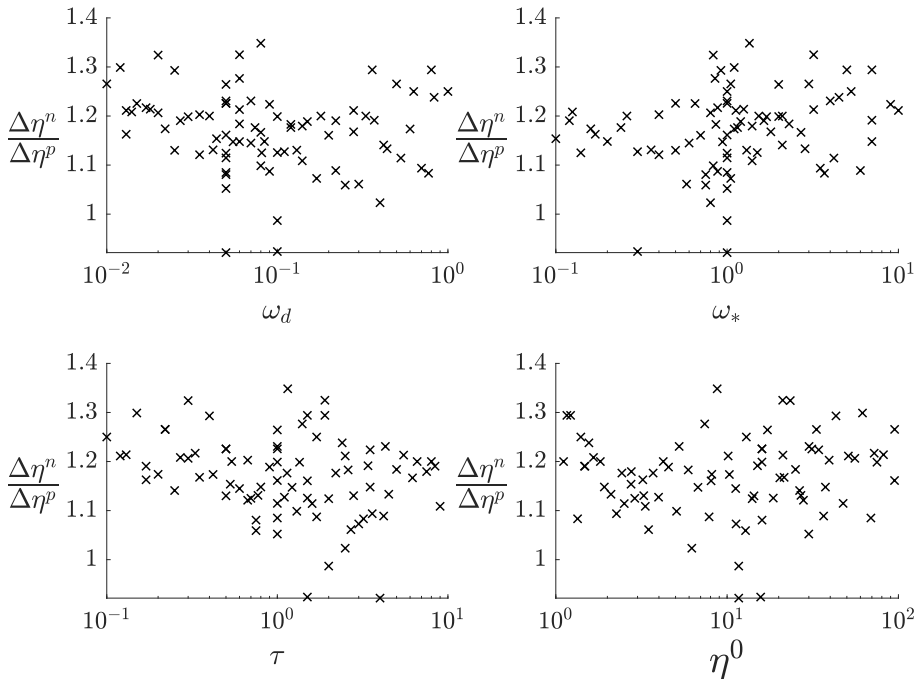


FIGURE 9. Dimits shift mismatch between the reduced mode prediction $\Delta\eta^P$ of Section 5 and what is observed in nonlinear simulations $\Delta\eta^n$ as a function of the configuration parameters ω_d , ω_* , τ , and η^0 . The prediction is generally seen to underpredict the actual shift by some 5-30% but otherwise remain consistent across configurations.

1999), and so we are therefore forced to settle for a flat decay in the absence of better alternatives. In principle the validity of the findings presented herein could cease to hold for other types of damping, since its inclusion would modify both the prediction and nonlinear Dimits shifts slightly. Nevertheless this seems to be an unimportant effect in so far as the matching between the two appears to remain mostly intact for reasonable hyperviscosities, and so we choose not to investigate this in any further detail.

6. Discussion

What has been demonstrated in this paper is that, through an appropriate asymptotic expansion, the moment hierarchy of gyrokinetics can self-consistently be closed at second order, resulting in a strongly driven gyrofluid system with both linear drive and nonlinear drift/zonal interactions. With the *ad hoc* introduction of additional damping, meant to encapsulate the effect of Landau damping, this system can be made to exhibit a Dimits shift. This Dimits shift corresponds to the point at which the zonal profile no longer can form a robustly tertiary stable staircase state which eventually is able to kill all drift waves.

Though similar, the transport bursts observed around the Dimits transition in this system are not strictly speaking the well-known zonal-driftwave predator-prey oscillations observed by e.g. Malkov *et al.* (2001) or Kobayashi *et al.* (2015), since the zonal energy typically only varies slightly during a drift wave burst. In spite of this steady zonal energy content, the zonal profile greatly varies during a burst, something which would

not be the case if they could trace their origin to the ferdinons recently discovered (van Wyk *et al.* 2016). Indeed, nothing resembling small-scale solitons are ever observed in our simulations. Instead it seems that these bursts trace their origin to the movement of tertiary unstable points as the zonal staircase is modified, combined with the fact that new localised tertiary modes take so long to emerge, being close to marginal stability within the Dimits regime.

Similarly to the prediction of St-Onge (2017), it is possible to employ a consistently and comparatively accurate estimate of when the Dimits transition should occur by approximating the full zonal profile with a single mode, if it is taken to be that mode which is most stabilising. Naturally the validity of such a simplification may not in general be taken for granted; one has to be reasonably sure that the system under consideration has small enough collisional damping and that other kinds of nonlinear behaviour do not dominate during the Dimits transition so that the tertiary instability is still of prime importance. If however the transition continues to coincide with a tertiary stability threshold, then one might, in more general systems, be able to approximate the typical zonal profiles with some reduced mode scheme, adapting equations (5.2)-(5.5) in some simple way, to maintain that computational simplicity that would make our theoretical method of Dimits shift estimation a practically useful and predictive tool. Because of this, future work aims to investigate whether this state of affairs holds for fully gyrokinetic systems.

7. Acknowledgements

This work has been carried out within the framework of the EUROfusion consortium and has received funding from the Euratom research and training programme 2014-2018 and 2019-2020 under grant agreement No 633053. The views and opinions expressed herein do not necessarily reflect those of the European Commission.

REFERENCES

- ABEL, I. G., PLUNK, G. G., WANG, E., BARNES, M., COWLEY, S. C., DORLAND, W. & SCHEKOCHIHIN, A. A. 2013 Multiscale gyrokinetics for rotating tokamak plasmas: fluctuations, transport and energy flows. *Reports on Progress in Physics* **76** (11), 116201, arXiv: 1209.4782.
- BARNES, M, PARRA, F I & SCHEKOCHIHIN, A A 2011 Critically Balanced Ion Temperature Gradient Turbulence in Fusion Plasmas. *Physical Review Letters* **107** (11), 115003.
- BEER, MICHAEL ALAN 1995 Gyrofluid models of turbulent transport in tokamaks. PhD thesis, Princeton University.
- BERIONNI, V & GÜRÇAN, Ö D 2011 Predator prey oscillations in a simple cascade model of drift wave turbulence. *Physics of Plasmas* **18** (11), 112301.
- CATTO, P J 1978 Linearized gyro-kinetics. *Plasma Physics* **20** (7), 719–722.
- CHOI, DUK-IN & HORTON, WENDELL 1980 Weakly localized two-dimensional drift modes. *Physics of Fluids* **23** (2), 356.
- CONNOR, J W & WILSON, H. R. 1994 Survey of theories of anomalous transport. *Plasma Physics and Controlled Fusion* **36** (5), 719–795.
- DIAMOND, P H, ITOH, S-I, ITOH, K & HAHM, T S 2005 Zonal flows in plasma—a review. *Plasma Physics and Controlled Fusion* **47** (5), R35–R161.
- DIF-PRADALIER, G, DIAMOND, P H, GRANDGIRARD, V, SARAZIN, Y, ABITEBOUL, J, GARBET, X, GHENDRIH, PH, STRUGAREK, A, KU, S & CHANG, C S 2010 On the validity of the local diffusive paradigm in turbulent plasma transport. *Physical Review E* **82** (2), 025401.
- DIMITS, A M, BATEMAN, G, BEER, M A, COHEN, B I, DORLAND, W, HAMMETT, G W, KIM, C, KINSEY, J E, KOTSCHENREUTHER, M, KRITZ, A H, LAO, L L, MANDREKAS, J, NEVINS, W M, PARKER, S E, REDD, A J, SHUMAKER, D E, SYDORA, R & WEILAND,

- J 2000 Comparisons and physics basis of tokamak transport models and turbulence simulations. *Physics of Plasmas* **7** (3), 969–983.
- FARRELL, BRIAN F & IOANNOU, PETROS J 2009 A stochastic structural stability theory model of the drift wave–zonal flow system. *Physics of Plasmas* **16** (11), 112903.
- FRIEMAN, E A 1982 Nonlinear gyrokinetic equations for low-frequency electromagnetic waves in general plasma equilibria. *Physics of Fluids* **25** (3), 502.
- HASEGAWA, AKIRA & MIMA, KUNIOKI 1978 Pseudo-three-dimensional turbulence in magnetized nonuniform plasma. *Physics of Fluids* **21** (1), 87.
- HASEGAWA, AKIRA & WAKATANI, MASAHIRO 1983 Plasma Edge Turbulence. *Physical Review Letters* **50** (9), 682–686.
- HORTON, WENDELL, CHOI, DUK-IN & TANG, W.M. 1981 Toroidal drift modes driven by ion pressure gradients. *Physics of Fluids* **24** (6), 1077.
- IVANOV, PLAMEN G, SCHEKOCIHIN, A A, DORLAND, W, FIELD, A R & PARRA, F I 2020 Zonally dominated dynamics and Dimits threshold in curvature-driven ITG turbulence , arXiv: 2004.04047.
- KADOMTSEV, B.B. & POGUTSE, O.P 1970 Turbulence in toroidal systems. In *Reviews of Plasma Physics* (ed. Leontonovich M.A.), , vol. 5, 1995, pp. 249–400. Boston, MA: Springer.
- KIM, CHANG-BAE, MIN, BYUNGHOO & AN, CHAN-YONG 2018 Localization of the eigenmode of the drift-resistive plasma by zonal flow. *Physics of Plasmas* **25** (10), 102501.
- KIM, CHANG-BAE, MIN, BYUNGHOO & AN, CHAN-YONG 2019 On the effects of nonuniform zonal flow in the resistive-drift plasma. *Plasma Physics and Controlled Fusion* **61** (3), 035002.
- KIM, EUN-JIN & DIAMOND, P H 2002 Dynamics of zonal flow saturation in strong collisionless drift wave turbulence. *Physics of Plasmas* **9** (11), 4530–4539.
- KINSEY, J. E., WALTZ, R. E. & CANDY, J. 2005 Nonlinear gyrokinetic turbulence simulations of E×B shear quenching of transport. *Physics of Plasmas* **12** (6), 062302.
- KOBAYASHI, SUMIRE, GÜRCAN, ÖZGÜR D & DIAMOND, PATRICK H 2015 Direct identification of predator-prey dynamics in gyrokinetic simulations. *Physics of Plasmas* **22** (9), 090702.
- KOBAYASHI, SUMIRE & ROGERS, BARRETT N. 2012 The quench rule, Dimits shift, and eigenmode localization by small-scale zonal flows. *Physics of Plasmas* **19** (1), 012315.
- KRAICHNAN, ROBERT H 1967 Inertial Ranges in Two-Dimensional Turbulence. *Physics of Fluids* **10** (7), 1417.
- LANDAU, LEV 1946 On the vibrations of the electronic plasma. *J. Phys. USSR* **10** (26).
- LI, JIACONG & DIAMOND, PATRICK H. 2018 Frictionless Zonal Flow Saturation by Vorticity Mixing , arXiv: 1809.09589.
- LIEWER, PAULETT C. 1985 Measurements of microturbulence in tokamaks and comparisons with theories of turbulence and anomalous transport. *Nuclear Fusion* **25** (5), 543–621.
- MAKWANA, K. D., TERRY, P. W., PUESCHEL, M. J. & HATCH, D. R. 2014 Subdominant Modes in Zonal-Flow-Regulated Turbulence. *Physical Review Letters* **112** (9), 095002.
- MALKOV, M A, DIAMOND, P H & ROSENBLUTH, M N 2001 On the nature of bursting in transport and turbulence in drift wave–zonal flow systems. *Physics of Plasmas* **8** (12), 5073–5076.
- MCMILLAN, B. F., HILL, P, BOTTINO, A, JOLLIET, S, VERNAY, T & VILLARD, L 2011 Interaction of large scale flow structures with gyrokinetic turbulence. *Physics of Plasmas* **18** (11), 112503.
- MISHCHENKO, ALEXEY, PLUNK, GABRIEL G. & HELANDER, PER 2018 Electrostatic stability of electron–positron plasmas in dipole geometry. *Journal of Plasma Physics* **84** (2), 905840201.
- NORDMAN, H., WEILAND, J. & JARMÉN, A. 1990 Simulation of toroidal drift mode turbulence driven by temperature gradients and electron trapping. *Nuclear Fusion* **30** (6), 983–996.
- PLUNK, G G, HELANDER, P, XANTHOPOULOS, P & CONNOR, J W 2014 Collisionless microinstabilities in stellarators. III. The ion-temperature-gradient mode. *Physics of Plasmas* **21** (3), 032112.
- PLUNK, G G, TATSUNO, T & DORLAND, W 2012 Considering fluctuation energy as a measure of gyrokinetic turbulence. *New Journal of Physics* **14** (10), 103030.
- QIAN, J 1986 Inverse energy cascade in two-dimensional turbulence. *Physics of Fluids* **29** (11), 3608.

- RATH, F., PEETERS, A. G., BUCHHOLZ, R., GROSSHAUSER, S. R., SEIFERLING, F. & WEIKL, A. 2018 On the tertiary instability formalism of zonal flows in magnetized plasmas. *Physics of Plasmas* **25** (5), 052102.
- ROGERS, B. N., DORLAND, W. & KOTSCHENREUTHER, M. 2000 Generation and Stability of Zonal Flows in Ion-Temperature-Gradient Mode Turbulence. *Physical Review Letters* **85** (25), 5336–5339.
- ROSENBLUTH, M. N. & HINTON, F. L. 1998 Poloidal Flow Driven by Ion-Temperature-Gradient Turbulence in Tokamaks. *Physical Review Letters* **80** (4), 724–727.
- RYTER, F., ANGIONI, C., GIROUD, C., PEETERS, A.G., BIEWER, T., BILATO, R., JOFFRIN, E., JOHNSON, T., LEGGATE, H, LERCHE, E, MADISON, G, MANTICA, P, VAN EESTER, D & VOITSEKHOVITCH, I 2011 Simultaneous analysis of ion and electron heat transport by power modulation in JET. *Nuclear Fusion* **51** (11), 113016.
- ST-ONGE, DENIS A 2017 On non-local energy transfer via zonal flow in the Dimits shift. *Journal of Plasma Physics* **83** (05), 905830504, arXiv: 1704.05406v3.
- SUGAMA, H. 1999 Damping of toroidal ion temperature gradient modes. *Physics of Plasmas* **6** (9), 3527–3535.
- TERRY, P W 2004 Inverse Energy Transfer by Near-Resonant Interactions with a Damped-Wave Spectrum. *Physical Review Letters* **93** (23), 235004.
- WALTZ, R. E., DEWAR, R. L. & GARBET, X. 1998 Theory and simulation of rotational shear stabilization of turbulence. *Physics of Plasmas* **5** (5), 1784–1792.
- VAN WYK, F, HIGHCOCK, E. G., FIELD, A. R., ROACH, C. M., SCHEKOCIHIN, A. A., PARRA, F. I. & DORLAND, W. 2017 Ion-scale turbulence in MAST: anomalous transport, subcritical transitions, and comparison to BES measurements. *Plasma Physics and Controlled Fusion* **59** (11), 114003, arXiv: 1704.02830.
- VAN WYK, F., HIGHCOCK, E. G., SCHEKOCIHIN, A. A., ROACH, C. M., FIELD, A. R. & DORLAND, W. 2016 Transition to subcritical turbulence in a tokamak plasma. *Journal of Plasma Physics* **82** (6), 905820609, arXiv: 1607.08173.
- ZHU, HONGXUAN, ZHOU, YAO & DODIN, I. Y. 2020a Theory of the Tertiary Instability and the Dimits Shift from Reduced Drift-Wave Models. *Physical Review Letters* **124** (5), 055002, arXiv: 1910.05227.
- ZHU, HONGXUAN, ZHOU, YAO & DODIN, I. Y. 2020b Theory of the tertiary instability and the Dimits shift within a scalar model. *Journal of Plasma Physics* **86** (4), 905860405.